

SLAC-PUB-4654  
March 1989  
(I/A)

**PRECISION MEASUREMENTS OF THE SLC SPECTROMETER  
MAGNETS\***

**MICHAEL LEVI**

*Lawrence Berkeley Laboratory, Berkeley, California 94720*

**JORDAN NASH**

*Stanford Linear Accelerator Center, Stanford, California 94309*

**STERLING WATSON**

*University of California at Santa Cruz, Santa Cruz, California 95064*

Precision laboratory measurements have been made of the SLC spectrometer magnets. The value of the magnetic field integral,  $\int B dl$ , has been determined in the laboratory to an accuracy of  $\delta \int B dl / \int B dl = \pm 0.7 \times 10^{-4}$ . Additionally, high-precision methods of monitoring the field integral of these magnets during actual operation have been developed. With these methods the absolute value of the field integral is continuously monitored to an accuracy of  $\delta \int B dl / \int B dl = \pm 1.0 \times 10^{-4}$ .

Submitted to *Nuclear Instruments and Methods A*.

---

\* Work supported in part by Department of Energy Contracts DE-AC03-76SF00098, DE-AC03-76SF00515, and DE-AM03-76SF00010.

## 1. Introduction

At the Stanford Linear Collider (SLC) [1], a precise, independent measurement of the electron and positron beam energies is essential to determine the mass and width of the  $Z^0$  resonance [2]. Precision spectrometers have been installed in both SLC extraction lines, in order to determine the energy of each beam,  $E_{beam}$ , at the interaction point to an accuracy of  $\delta E_{beam}/E_{beam} = \pm 3 \times 10^{-4}$ .

The conceptual design of the extraction line spectrometer [3] is as follows: After passing through the interaction point, the beam bunches are transported through the SLC final focus system [4] and ejected from the main line with a pulsed kicker and septum magnets into the extraction line. Each extraction line consists of a series of quadrupole and dipole magnets which guide the beam through the spectrometer magnet, B32. This is an accurately measured dipole magnet which bends the beam by an amount inversely proportional to the beam energy. Smaller dipole magnets located before and after the main bend magnet create two bands of synchrotron light with a separation proportional to the bend angle. Synchrotron light detectors placed at the focal point defined by the quadrupoles measure the displacement ( $d$ ) between these swaths. The energy of the beam is determined from the displacement, the field integral ( $\int B dl$ ), and the distance between B32 and the detectors ( $L$ ), as shown in eq. (1) below:

$$E_{beam} [eV] = c \cdot \left( \frac{L}{d} \right) \int B dl [T \cdot m] , \quad (1)$$

where  $d \approx 0.27$  m and  $L \approx 15$  m. A conceptual drawing of the south (electron) extraction line is shown in fig. 1. The north (positron) line is similar in design.

To implement this design, a spectrometer magnet with a very uniform field has been designed and built at Stanford Linear Accelerator Center. The magnet has a very wide gap— $228.6 \times 31.7$  mm (width  $\times$  height)—to simultaneously accommodate both the electron beam and the magnetic field monitoring devices (see fig. 2). Beam energies are expected to be between 42 and 50 GeV, with a maximum design

energy of 55 GeV. The specified bend angle through the spectrometer magnet is 18.286 mrad, requiring a field integral of  $3.050 \text{ T} \cdot \text{m}$  at 50 GeV. The iron core magnet (C1008 steel) has a 2.54 m effective length and a typical pole field of 1.200 T provided by two 16-turn, 865-amp, copper, water-cooled saddle coils. Mirror end plates are installed on each magnet to contain fringe fields. Two magnets have been constructed, B32S for installation in the south (electron) extraction line and B32N for installation in the north (positron) extraction line.

The two spectrometers are accurately mapped in the laboratory under a variety of conditions that might be expected during operation and transferable monitoring standards are calibrated for each magnet. The two laboratory methods are discussed in sec. 2, the monitoring standards in sec. 3 and operational performance in sec. 4.

## 2. Laboratory field mapping

Two independent, high-precision methods have been developed to measure the field integral and field shape of the magnets. Both methods have an expected mapping accuracy of better than 60 ppm (parts per million). Throughout this paper ppm will be used for the ratio of the error in a measurement to the actual measurement. Both methods are used in order to determine an overall systematic error and to increase confidence in the measurements. These techniques are described below.

### 2.1 *Moving wire technique*

The first absolute measurement of the field integral discussed here is the “moving wire” technique. In this method, a wire is passed through the magnet gap and returned outside of the magnet to form a closed loop. A ribbon pack of 10, 100- $\mu\text{m}$  diameter, copper wires form the interior leg of a 10-turn loop [5]. Transverse motion of the wire pack in the magnetic field induces a voltage in the loop. From a precise measurement of the voltage integral and distance moved, the magnet

strength is then determined from eq. (2) below.

$$\int B dl [T \cdot m] = \frac{-\int V dt [V \cdot s]}{N \Delta x} \quad . \quad (2)$$

Here,  $\int V dt$  is the time integral of the induced voltage,  $N$  is the number of turns and  $\Delta x$  is the distance moved in meters.

The wires are secured in place at either end by wire holders at a tension of 1.5 Nt. The holders are mounted on precision traveling stages [6]. The wire pack is aligned to be parallel to the long axis ( $z$ ) of the magnet to an accuracy of 1 mrad. The loop is then completed outside of the magnet by a flexible cable. Both stages are aligned with the direction of travel parallel to the  $x$ -axis to a precision of 4 mrad, where the  $x$ -axis is perpendicular to both the  $z$ -axis and the magnetic field lines (the  $y$ -axis). This alignment error leads to an error on the field integral of 8 ppm. Both stages are mounted equidistant from the magnet center, 70.1 cm from the magnet end-plates. The  $y$  position of the stages can also be adjusted. These stages have 250 mm of travel and can be driven in 1- $\mu$ m steps at speeds up to 3 mm/sec. Stage positions are monitored by built in optical encoders which count lead screw rotations and are read through CAMAC. Roll, pitch and yaw are less than 0.02 mrad for this stage. The stage position accuracy is better than 30 ppm over the full range of travel. This is checked by mounting a laser retroreflector (corner cube prism) on the wire holder, setting up a laser interferometer system [7], and comparing the interferometer reading with that of the optical encoder. The interferometer has an absolute accuracy better than 1 ppm with automatic compensation for air temperature, pressure and humidity. In a measurement, both ends of the wire are moved simultaneously through a ramp up, steady speed and ramp down cycle to smoothly cover the distance desired (typically 10 mm). The actual speed affects the voltage induced but not the voltage integral, which depends only on the total distance moved. A system block diagram is shown in fig. 3.

The voltage is read by an HP 3457A Digital Voltmeter (DVM). In this application, the DVM performs a series of readings with an analog integration period of 16.6666 msec synchronously to a 50 Hz clock. Under these conditions the absolute accuracy of the DVM is 25 ppm. The external time base is based on a temperature stabilized quartz oscillator with a long-term accuracy of 2 ppm. Both the DVM and the time base are calibrated against NBS traceable standards. For each measurement, the DVM is set up to take a series of readings and is then triggered by the external clock. A typical waveform is shown in fig. 4. A series of measurements, five where the stages move in the positive  $x$  direction and five in the negative  $x$  direction, allows for detection and cancellation of any DC offset level and estimation of the repeatability of the technique. During measurements, the field from an NMR probe placed in a fixed position in the magnet and the magnet current are recorded. This corrects for drifts in the magnet current during a measurement and permits comparisons between measurements taken at different times. The mean standard deviation on all sets of ten measurements is  $\delta \int B dl / \int B dl = \pm 28$  ppm. This is an indication of the short-term repeatability of this method. Estimated systematic errors for the "moving wire" method are summarized in table 1.

Table 1  
Systematic errors for "moving wire" method

| Error Source                   | Error (ppm) |
|--------------------------------|-------------|
| Distance determination (stage) | 30          |
| Misalignment of travel         | 8           |
| DVM accuracy                   | 25          |
| Time base                      | 2           |
| Combined systematic error      | 40          |

With this technique, measurements of the magnet quality are performed. Prior to the first measurement of the magnet, and performed only once during its service, the magnet is "conditioned" by running the magnet into saturation at 1500 amps. Prior to any series of measurements the magnet is "standardized" by ramping

the current through a controlled cycle. Three cycles of ramping from 1050 amps to 30 amps and back to 1050 amps at 20 amps/sec establishes a high degree of repeatability in the field.

The first measurements of each magnet are excitation curves of the magnet. The current is ramped from 1000 amps to 600 amps in 10-amp increments. At each step the field integral is measured. The data are shown in fig. 5. The excitation curves are used to establish current settings for a desired field strength in the following studies.

The field uniformity across the gap is an important magnet quality because the beam position through B32 can vary by  $\pm 3$  mm in  $x$  due to sagitta and by a similar amount due to beam steering. The field symmetry about the  $y-z$  plane is also important because the ideal trajectory of the beam is at  $x = -32$  mm while the field monitoring devices are located at  $x = +32$  mm. For this reason, measurements are made across the gap to well beyond the regions of interest [ $x = (-100 \text{ mm} \dots +100 \text{ mm})$ ] at currents corresponding  $E_{beam} = (42, 44, 46, 48, 50, 55 \text{ GeV})$ . In these measurements, the stages are moved in 10-mm steps. Field integral maps of B32N and B32S are shown in fig. 6 with the measurements normalized to 1.0 over the central region. The measurements at 55 GeV are beyond the expected operating range of SLC but are included here for completeness. Here, the effects of magnet saturation at 55 GeV are clearly seen but the field shape is quite symmetrical and uniform to  $\delta \int B dl / \int B dl = \pm 41 \text{ ppm}$  (north) and  $\pm 54 \text{ ppm}$  (south) in the region occupied by the beam [ $\pm 10$  mm about nominal  $(x, y)$  beam position]. Variations in strength with  $x$  and  $y$  are shown in fig. 7 at 46 GeV.

When the two stages are moved in opposing directions, the induced voltage ( $V'$ ) is proportional to the offset of the magnetic center from the geometric center of the magnet and is given by eq. 3 below:

$$\Delta z = \frac{l}{2} \frac{\int V' dt}{\int V dt} , \quad (3)$$

where  $\Delta z$  is the offset of the magnetic center,  $l$  is the separation between wire holders, and  $\int V dt$  is the voltage integral measured with both stages moving in the same direction. The data show that the magnetic center of the magnets are within 0.7 mm of the geometric center for both magnets B32S and B32N.

## 2.2 *Moving probe technique*

The second absolute measurement technique, "moving probe," measures the field integral by driving an NMR probe [8] and a Hall probe [9] along the length of the magnet in small steps. In this manner the magnet strength is determined by summing over the measurements of the magnet using the trapezoid rule —  $\int B dl = \sum [(B_i + B_{i-1})/2] dl_i$ . The  $B_i$  are the field measurements at each point and  $dl_i$  is the step size. The probes are mounted with a laser retroreflector on a rail assembly which runs through the magnet and uses the laser interferometer to measure the probe position. The NMR probes are custom made, radiation hardened [10], miniature probes (Model 1065) attached to the probe electronics by a flexible shielded cable. Absolute accuracy for the NMR system is 10 ppm. The Hall effect probe is used in the fringe field of the magnet. This probe has a precision of 300 ppm and is calibrated during measurements by the NMR system in the region where both operate. Unlike the NMR probe, the Hall probe is sensitive to rotations. The maximum possible tilt (40 mrad), given the rigidity of the probe holder, would result in an error of 800 ppm. However, the Hall probe only measures 6% of the total field integral so the maximum expected contribution to the error is 48 ppm.

The field map measured by the NMR and Hall probes is initiated at a location 28 cm beyond the end of the magnet where the measured field due to the magnet is much less than the Earth's ambient field. A schematic diagram of the mapping system is shown in fig. 8. The mapping procedure is as follows: First, the rail assembly is installed in the desired  $x, y$  starting location. The laser interferometer is aligned to be parallel to the length of the magnet to within 0.5 mrad. The precise starting location along  $z$  for each map is determined by locating a registration mark

on the Hall probe with respect to the geometrical center of the magnet. This is done to an accuracy of better than  $100 \mu\text{m}$ . A stepping motor drives the probes on a lead screw in steps ranging from  $100 \mu\text{m}$  to 1 cm depending on the value of  $d^2B(z)/dz^2$ . Smaller steps are taken where necessary to reduce the error in the field integral due to nonlinearities in the field shape to less than 10 ppm while allowing a complete field map in approximately 20 minutes. Representative maps are shown in fig. 9. The short-term repeatability of this method is quite good ( $\delta \int Bdl / \int Bdl = \pm 15 \text{ ppm}$ ). Table 2 summarizes the estimated systematic errors with this technique.

Table 2  
Systematic errors for "moving probe" method

| Error Source                                 | Error (ppm) |
|--|-------------|
| Position determination (laser)               | 1           |
| Misalignment of laser to beam path           | 0           |
| NMR system                                   | 10          |
| Hall probe precision (300 ppm $\times 6\%$ ) | 18          |
| Hall probe tilt (800 ppm $\times 6\%$ )      | 48          |
| Linear interpolation                         | 10          |
| Combined systematic error                    | 53          |

### 2.3 Measurement consistency

The values of the field integral from each method are now compared. The expected systematic error of the "moving wire" method is found in sec. 2.1 to be  $\delta \int Bdl / \int Bdl = \pm 40 \text{ ppm}$  with a statistical repeatability of  $\delta \int Bdl / \int Bdl = \pm 28 \text{ ppm}$ . For the "moving probe" method, the expected systematic error is  $\delta \int Bdl / \int Bdl = \pm 53 \text{ ppm}$  with a statistical repeatability of  $\delta \int Bdl / \int Bdl = \pm 15 \text{ ppm}$ . Within the precision of the two techniques both methods can be compared.

As part of the calibration procedure for each magnet, measurements of  $\int Bdl$  are made at the beam location and the monitor location at six different excitations,

with both techniques. In fig. 10, the difference between the two techniques is plotted as a function of beam energy at the two specified locations for each magnet. The mean difference between these techniques is 72 ppm with a point to point variation of 53 ppm. The agreement between the two absolute techniques is within the level expected due to the known systematic errors of the two techniques.

### 3. Field monitoring techniques

The absolute measurements are used to simultaneously calibrate three independent, transferable standards for monitoring the field strength: (1) a rotating "flip coil," (2) three stationary NMR probes and (3) a current transductor [11]. These methods allow the field integral to be monitored while the magnet is installed in the beam line.

#### 3.1 *Flip coil*

The flip coil consists of a rod of fused silica quartz 2.80 m long and 15 mm in diameter (see fig. 11). Quartz is used for several reasons: (1) radiation hardness to  $> 10^8$  Gy, (2) low thermal expansion coefficient of  $5.5 \times 10^{-7}/^{\circ}\text{C}$ , and (3) high mechanical strength. A ten-wire coil pack is wrapped once around the rod lengthwise, tensioned, and epoxied in place on flats ground along the length of the rod. This coil package is interconnected to provide a continuous ten-turn loop. Four cylindrical bearings support the rod in a section of aluminum channel stock. An AC synchronous motor rotates the coil at 3 rpm and the entire assembly is inserted in the magnet gap. The voltage induced by the changing flux is connected by a brush and slip ring assembly to the DVM system. Four flip coils were built to insure that spares exist. The time integral of the voltage ( $\int V dt$ ) over a half-wave-form will be proportional to the magnet strength according to the relationship:

$$\int B dl [T \cdot m] = \frac{-\int V dt [V \cdot s]}{N (2 \cdot d)} , \quad (4)$$

where  $d$  is the effective diameter of the coil and  $N$  is the number of turns in the coil. A passive, low pass filter ( $R = 3.9 \text{ k}\Omega$ ,  $C = 10 \mu\text{F}$ ) was used to remove

high-frequency noise sources. The filter reduces the signal by 75 ppm. A sample waveform is shown in fig. 12.

The field monitors are calibrated by correlating the monitor measurements with the absolute measurements done simultaneously at each magnet excitation. The data is then fit to the lowest order polynomial function [eq. (5) below] which yields acceptably small fit residuals for  $\Delta = |(\int B dl_{fit} - \int B dl_{meas}) / \int B dl_{meas}|$  ( $\Delta < 100$  ppm):

$$B(x) = (a_0 + a_1 x + a_2 x^2 + a_3 x^3 + a_4 x^4 + a_5 x^5) \times (1 + C_T \cdot \Delta T) \quad . \quad (5)$$

Here,  $B(x)$  is the magnet strength (in  $T \cdot m$ ) as function of the monitor value,  $x$ , and the difference from nominal temperature,  $\Delta T$ . For the flip coil,  $x$  is the voltage integral (typically 0.7 Volt  $\cdot$  sec). The  $a_i$  are the fit coefficients. The thermal coefficient ( $C_T$ ) is determined by reducing the flow of cooling water to the magnet and thus elevating the temperature. As the temperature increases, all magnet dimensions are expected to increase by 12 ppm/ $^{\circ}$ C, thus affecting the shape and strength of the magnetic field. The flip coil is expected to be insensitive to temperature changes. Comparison of the monitors with the absolute standards at low ( $27^{\circ}$ C) and high ( $35 - 40^{\circ}$ C) temperatures determines  $C_T$ . For the flip coils,  $C_T = 2.0 \pm 0.6$  ppm/ $^{\circ}$ C.

Each flip coil is calibrated in each magnet at six excitations (42 ... 55 GeV) using both the “moving wire” and “moving probe” standards. A second-order polynomial fit is sufficient to fit the data well for all coils. The average fit residual is 20 ppm with the “moving wire” data and 48 ppm with the “moving probe” data. In the final calibration, the “moving wire” data is used because of the better fit and better absolute accuracy. Figure 13 shows the fit error as a function of excitation for magnet B32S. In table 3, the fit coefficients and the fit residuals are summarized for each coil in each magnet.

In table 4, the estimated systematic errors with the flip coils are shown, excluding absolute calibration error. The dominant error for this method is the accuracy

Table 3  
Flip coil fit coefficients

| Magnet | Coil # | $a_2$      | $a_1$     | $a_0$      | Fit Residual<br>( $\times 10^{-6}$ ) |
|--------|--------|------------|-----------|------------|--------------------------------------|
| B32S   | 1      | -0.0029606 | 3.8608549 | -0.0016897 | 20                                   |
| B32S   | 2      | +0.0023479 | 3.4892518 | +0.0016397 | 19                                   |
| B32S   | 3      | +0.0073821 | 3.4264566 | +0.0056985 | 33                                   |
| B32S   | 4      | -0.0022167 | 3.4301264 | -0.0009844 | 17                                   |
| B32N   | 1      | -0.0013264 | 3.8584537 | -0.0009194 | 20                                   |
| B32N   | 2      | -0.0021434 | 3.4969237 | -0.0017916 | 11                                   |
| B32N   | 3      | +0.0003052 | 3.4386015 | +0.0003334 | 25                                   |
| B32N   | 4      | -0.0032493 | 3.4327610 | -0.0026126 | 14                                   |

of the DVM (35 ppm) in measuring the induced voltages. A typical 1 mrad misalignment of the flip coil would contribute 1 ppm to the measurement error. The error contributed by the uncertainty on  $C_T$  for a 15°C temperature rise is 9 ppm. Short-term repeatability is measured to be  $\sigma = 28$  ppm.

Table 4  
Systematic errors for flip coil

| Error Source              | Error (ppm) |
|---------------------------|-------------|
| DVM accuracy              | 35          |
| Time base                 | 2           |
| Misalignment of flip coil | 1           |
| Average fit error         | 20          |
| Thermal effects           | 9           |
| Combined systematic error | 42          |

### 3.2 NMR probes

The second monitoring method uses the readings from a set of three NMR probes installed in the flip coil support structure. These probes are located at the center of the magnet and 50 cm from either end. Due to the limited space

available, the probes are custom manufactured, miniature MetroLab probes as described previously. Accurate measurements at specific points are possible with this technique, but not a direct measurement of  $\int Bdl$ . The field integral must be inferred from a cross-calibration. Therefore, this technique is sensitive to magnet saturation effects and thermally induced geometry changes. Calibration of the NMR probes is similar to the flip coils but with "moving wire" data taken at 40 different excitations from 1000 to 600 amps because of the expected sensitivity to saturation effects. A second-order fit is used except for the central NMR probe in magnet B32N which has a small field inhomogeneity in this region and requires a third-order fit. In fig. 14, the fit results are shown. The mean fit residual here is 42 ppm when fit to the "moving wire" measurements. Table 5 shows the fit coefficients.

Table 5  
NMR probe fit coefficients

| Magnet | Probe | $a_3$      | $a_2$      | $a_1$     | $a_0$      | Fit Error<br>(ppm) |
|--------|-------|------------|------------|-----------|------------|--------------------|
| B32S   | 1     | 0.00       | -0.0063204 | 2.5734729 | -0.0071273 | 17                 |
| B32S   | 2     | 0.00       | -0.0594700 | 2.6748862 | -0.0587324 | 45                 |
| B32S   | 3     | 0.00       | -0.0151172 | 2.5874422 | -0.0141318 | 24                 |
| B32N   | 1     | 0.00       | +0.0061404 | 2.5440368 | +0.0092323 | 46                 |
| B32N   | 2     | -0.1969876 | +0.6078394 | 1.9373721 | +0.2108732 | 75                 |
| B32N   | 3     | 0.00       | -0.0120632 | 2.5785659 | -0.0099529 | 46                 |

Systematic errors for the NMR probes include the NMR system accuracy (10 ppm) and a typical 1-mm uncertainty in probe position (20 ppm). The average fit error is 42 ppm. The NMR probes have a much larger thermal coefficient ( $C_T = 12.5 \pm 2 \text{ ppm}/^\circ\text{C}$ ) than the flip coils due to the expansion coefficient of steel and the error in this results in a 30 ppm error on  $\int Bdl$  for a  $15^\circ\text{C}$  temperature rise. Estimates of this error come from the variations in multiple measurements of  $C_T$ . These errors are summarized in table 6. Short-term repeatability with this method is measured to be 5 ppm.

Table 6  
Systematic errors for NMR probes

| Error Source              | Error (ppm) |
|---------------------------|-------------|
| NMR system                | 10          |
| Probe position            | 20          |
| Average fit error         | 42          |
| Thermal effects           | 30          |
| Combined systematic error | 57          |

### 3.3 Current monitors

The final method of determining the field integral is to monitor the current flowing in the magnet conductor with a transductor which transforms the DC current flow into a DC voltage without electrical connection to the power supply system. The rated relative precision of this device is 100 ppm with an output of 5 volts per 1000 amps. When the standardization cycle described previously is followed, the measured current correlates moderately well with the true field integral. Calibration is performed as for the other monitors. Due to the onset of magnet saturation at higher excitations, the field integral was a nonlinear function of the current and required a fifth or sixth order fit with a worst case fit residual of 75 ppm. The fit coefficients for the transductor are shown in table 7 and the fit results are seen in fig. 15. Table 8 summarizes the estimated systematic errors for this method. At typical currents, the error from the DVM is 40 ppm. The thermal coefficients derived for the transductors have large uncertainties ( $C_T^N = -31 \pm 8 \text{ ppm/}^\circ\text{C}$ ,  $C_T^S = -26 \pm 7 \text{ ppm/}^\circ\text{C}$ ) which lead to errors on the field integral of 120 ppm for a  $15^\circ\text{C}$  temperature rise. Additionally, it is found that the recent magnetic history of the magnet can significantly affect the field integral, causing errors up to 65 ppm. External magnetic fields and mechanical misalignments of the current bus can alter the magnetic properties and thus the absolute calibration of the transductor. Therefore, moving the transductor from the laboratory to the field can induce large changes but they shouldn't affect the relative precision of this

method. This error is not included in the listed systematic errors. The short-term repeatability with this technique is 16 ppm.

Table 7  
Transductor fit coefficients

| Magnet                 | B32S    | B32N    |
|------------------------|---------|---------|
| $a_6(\times 10^{-18})$ | -1.455  | -2.149  |
| $a_5(\times 10^{-15})$ | +2.481  | +3.233  |
| $a_4(\times 10^{-13})$ | -6.018  | +4.478  |
| $a_3(\times 10^{-9})$  | -0.615  | -1.904  |
| $a_2(\times 10^{-7})$  | +4.658  | -8.570  |
| $a_1(\times 10^{-3})$  | 4.3419  | 5.1762  |
| $a_0$                  | -0.1997 | -0.4375 |
| Fit error (ppm)        | 33      | 75      |

Table 8  
Systematic errors for transductors

| Error Source              | Error (ppm) |
|---------------------------|-------------|
| Transductor system        | 100         |
| DVM                       | 40          |
| Fit error                 | 75          |
| Thermal effects           | 120         |
| Magnet history            | 65          |
| Combined systematic error | 190         |

### 3.4 Study of systematic errors

Measurements of the repeatability of each of the monitors are performed under a variety of conditions: (1) swapping the DVM's used for reading voltages, (2) inserting the aluminum beam pipe in the magnet gap, (3) switching filters on the flip coil signal, (4) operating with the magnet rolled 90° (which occurs in the south extraction line) and (5) comparing measurements taken on separate days. None of these variations caused a statistically significant effect with the exception

of measurements on different days. For the flip coils, the variation with respect to the absolute standards is  $\delta \int B dl / \int B dl = 44$  ppm. For the NMR probes and the transductors the variations are 86 ppm and 84 ppm, respectively. This gives an estimate of the long-term repeatability of each monitoring method.

#### 4. Operation and conclusion

Following the completion of all laboratory magnetic measurements, the spectrometer magnets were installed in the north and south extraction lines along with the other beam line components necessary for operation of the extraction line spectrometer.

##### 4.1 *Installation*

Flip coils are installed in each magnet and the field strength is measured at the monitor and beam locations ( $x = \pm 32$  mm) to recheck the magnet uniformity. The flip coils are then mounted securely in the precise location used during the laboratory calibration. The signals are transmitted on 300-m-long, shielded, twisted pair cables from the beam line to the DVM location. Magnet currents, voltage drops and temperatures are also monitored by the DVM. One NMR probe is installed in each magnet. The high-frequency ( $\approx 50$  MHz) NMR signal is transmitted 300 m over a low-loss, video-quality cable with filters and isolation transformers to reduce noise from the accelerator to acceptable levels. The complete system is controlled by a Macintosh II computer with an IEEE-488 interface and software drivers [12].

##### 4.2 *Operation of magnets and monitors*

With the magnets in operation, the performance of the magnets and the monitors are investigated. Several items are checked: (1) the stability of the power supply current and the magnet temperature, (2) the stability and precision of the various monitors, (3) the temperature dependance of the monitors and (4) the absolute agreement between the monitors of the field integral. Over periods of many hours, the current measured by the transductor is stable to 50 ppm (fig. 16). The temperatures of the magnets installed in the beam line are typically 36°C after

reaching thermal equilibrium. A temperature history plot is shown, starting from when the power supply is turned on until equilibrium is reached. Data from the flip coils and the NMR probes show that the short-term relative precision is very good. These plots show changes in magnet strength which are strongly correlated with the temperature changes. These correlations reflect the relative temperature coefficients of the various monitors.

The absolute agreement between the monitors of the value of  $\int B dl$  is also determined. Figure 17 shows a comparison between the field integral determined by the flip coil and the NMR probe and transductor over a period of several months. The mean difference between the flip coils and the NMR probes is  $-52 \pm 24$  ppm (north) and  $27 \pm 10$  ppm (south), while for the transductor it is  $532 \pm 68$  ppm (north) and  $434 \pm 53$  ppm (south). The large error with the transductor is due to magnetic and mechanical differences in the installation environment. Also, an excitation curve of the north and south spectrometer magnets is taken by standardizing the magnets and ramping down to the desired excitations over the range of  $3.40 [T \cdot m] > \int B dl > 2.40 [T \cdot m]$ . A plot of the difference between the flip coil measurement and the other two magnet monitors is shown in fig. 18 for magnet B32S. The NMR and flip coil track together well although the NMR differs from the flip coil by  $\delta \int B dl / \int B dl = -17 \pm 43$  ppm (north) and  $+32 \pm 15$  ppm (south). The disagreement between these techniques is consistent with the expected errors.

#### 4.3 Conclusion

Overall accuracy of the complete monitoring system can now be evaluated. Table 9 summarizes the known contributions to errors in the measurement of the field integral for each monitoring method. The absolute error is from the uncertainty in the absolute measurements given in sec. 2.3. Uniformity is the error due to changes in the field strength at different transverse locations given in sec. 2.1, while survey errors are from misalignments of the magnet relative to the beam. A maximum misalignment of 2.0 mrad is assumed for all angles from the survey of the beam line, which results in an error of 4 ppm. The relative error is the

systematic error for each monitoring technique, determined previously. Adding all these errors in quadrature yields the combined error. The mean error is defined here as mean difference between the flip coil measurement and the other methods for a series of measurements taken at various magnet excitations.

Table 9  
Summary of errors in monitors of  $\int B dl$

| Error Source           | Flip Coil<br>(ppm) | NMR<br>(ppm) | Transductor<br>(ppm) |
|------------------------|--------------------|--------------|----------------------|
| Absolute               | 72                 | 72           | 72                   |
| Uniformity             | 54                 | 54           | 54                   |
| Survey                 | 4                  | 4            | 4                    |
| Relative               | 42                 | 57           | 190                  |
| Combined               | 100                | 110          | 210                  |
| Mean error             | —                  | 25           | 331                  |
| Precision (short-term) | 28                 | 5            | 16                   |

In summary, several absolute and relative measurement techniques for determining the  $\int B dl$  of a dipole magnet have been developed. Measurements with these methods have determined the field quality and strength of the SLC spectrometer magnets to an extremely high accuracy over a wide variety of operating conditions. The accuracy of these techniques has been determined and the relative monitoring methods have been calibrated with the absolute standards. Combining all sources of errors results in a total error on the measurement of the field integral, by the best monitor, of 100 ppm. This includes all known systematic errors and the measurement precision.

### Acknowledgements

We would like to acknowledge the substantial support of Martin Terman in the development of measurement software and analysis of the properties of these magnets. We would also like to acknowledge the help of William Brunk and Dieter Walz for the design and engineering of magnets, and Michael Lateur for the design

and construction of the flip coils. Joe Cobb, Dave Jenson, Jussi Oijala, and Dan Jones are thanked for their assistance with the magnetic measurements and for graciously allowing us to use their laboratory. Finally, we would like to acknowledge Bernie Denton and Ed Keyser for insuring the smooth installation of the spectrometer magnets. Without the help of these people the design, construction, measurement and installation of the spectrometer magnets would not have been possible.

## REFERENCES

1. B. Richter and R. Stiening, *1987 International Symposium on Lepton and Photon Interactions at High Energy*, North-Holland, eds. W. Bartel and H. Ruckl, Hamburg (1987) p. 495;  
and SLAC Linear Collider Conceptual Design Report, SLAC-299 (1980).
2. J. Dorfan, "New Frontiers in Particle Physics," *World Scientific*, eds. J. Cameron, B. Campbell, A. Kamal and F. Khanna (1986) p. 82.
3. Mark II Collaboration and SLC Final Focus Group, SLAC-SLC-PROP-2 (1986).
4. R. A. Erickson, *U.S. Summer School on High Energy Particle Accelerators*, ed. R. Learner, AIP Conference Proceedings, No. 184 (1989).
5. The wire pack is multifilar magnet wire B (10) 381191 manufactured by MWS Wire Industries. The ten wires are bonded together to form a flat ribbon pack approximately 0.1 mm by 1.0 mm.
6. The Klinger MT-160 is a precision, stepping motor driven, translation stage. with internal optical encoder.
7. Hewlett Packard HP 5526 Laser Interferometer system. Measures distances and velocities up to a distance of 200 m with an accuracy of 0.7 ppm.
8. The NMR system is a MetroLab 3020 Teslameter with associated amplifier/multiplexer (Model 2031) and Model 1065 probes. Absolute accuracy is better than 10 ppm and relative precision is better than 1 ppm. Automatic search and NMR lock over full probe range (0.7-2.1 Tesla).
9. The Hall probe is a Group 3 Model DTM-141 system with temperature compensated probes.
10. Robert Openshaw, TRIUMF, private communication. Replacement of one bipolar transistor with a JFET increases the radiation hardness by a factor of ten.

11. G. E. Fischer, SLAC-PUB-3726 (1985).
12. National Instruments NB-GPIB Interface card and NI-488 software.

## FIGURE CAPTIONS

- 1) Conceptual design of the extraction line spectrometer. The quadrupole doublet focuses the beam at the plane of the synchrotron monitors. The horizontal bending magnets generate synchrotron light used to measure the bend angle of the vertical analysing bend.
- 2) Cross-sectional view of magnet B32 showing location of  $e^\pm$  beam, the synchrotron light ( $\gamma$ -rays) and magnetic field monitors.
- 3) System block diagram for "moving wire" technique. The PC controls and monitors the stages while measuring the induced voltage integral with the DVM.
- 4) Typical "moving wire" waveform. The field integral is proportional to the voltage integral of this waveform.
- 5) Saturation curves for the spectrometer magnets. Saturation is defined here as: Saturation =  $1 - K \int Bdl/I$ , where  $I$  is the magnet current and  $K$  is the proportionality of  $\int Bdl$  to  $I$  at 600 amperes excitation; (a) B32 north, (b) B32 south.
- 6) Magnetic field integral maps across the magnet gap as a function of  $x$  in 10-mm steps, using the "moving wire" technique. The solid curve is at an excitation corresponding to 46 GeV beam energy. The other curves show the uniformity of the magnets at various magnet excitations. The arrows indicate the locations of the beam and the field monitors; (a) B32 north, (b) B32 south.
- 7) Field integral maps across gap as a function of  $x$  for three  $y$  positions ( $y = 0, \pm 10$  mm); (a) B32 north, (b) B32 south.

- 8) System block diagram for the “moving probe” technique. A Hall probe and NMR probe measure the magnetic field while the probes are stepped through the magnet. The probe position is monitored by a laser interferometer. A detail of the probe holder shows the mounting of the probes with the laser retroreflector.
- 9) Typical “moving probe” maps of the magnetic field as a function of  $z$ ; (a) B32 south (full scale), (b) B32 south with expanded vertical scale to show uniformity, (c) B32 north.
- 10) Difference between the “moving wire” and “moving probe” measurement techniques at various magnet excitations. Data is taken at the beam ( $x = -32$  mm) and at the monitor ( $x = +32$  mm) positions. The offset and statistical scatter in these data points are good indicators of accuracy and precision of the measurement techniques; (a) B32 north, (b) B32 south.
- 11) Drawing of flip coil showing quartz rod, coil pack, support structure, and drive system. The coil pack is epoxied in place on the quartz rod and the loop is connected to the slip ring assembly to permit continuous rotation. The motor rotates the coil assembly at 3 rpm. Holders for the NMR probes allow three probes to be installed in the completed assembly without interfering with the flip coil.
- 12) Typical flip coil waveform. The field integral is proportional to the integral over a half-cycle of the waveform. The rotation speed is 6 rpm for this waveform.
- 13) Fit residuals for flip coils as a function of excitation for magnet B32S. The quantities plotted here are the residuals in ppm between the data being fitted and the actual fit. Residuals for “moving wire” data compared to the flip coil are shown.
- 14) Fit residuals for NMR probes in magnet B32S. The residual between the data and the fit are shown.

- 15) Fit residuals for the current transductor on magnet B32S.
- 16) Typical history plots of various magnet monitors for magnet B32 south. Data is taken at ten minute intervals: (a) Temperature history plot showing the exponential rise and fall of the temperature. The equilibrium temperature depends on magnet current and cooling water temperature and flow; (b) History plot of the magnet current measured by the current transductor shows the magnets going from off to on twice; (c) Flip coil history plot. The voltage integral as measured by the flip coil is shown here. Short term fluctuations are small but significant long term variations correlated with the temperature changes are present; (d) NMR probe history plot.
- 17) The difference between the flip coil and the other monitors of field strength is shown over a period of several months. The vertical scale shows the difference between the NMR probe and current transductor compared to the flip coil.
- 18) Difference between the flip coil compared with the NMR probe and with the current transductor at various excitations; (a) B32 north, (b) B32 south.

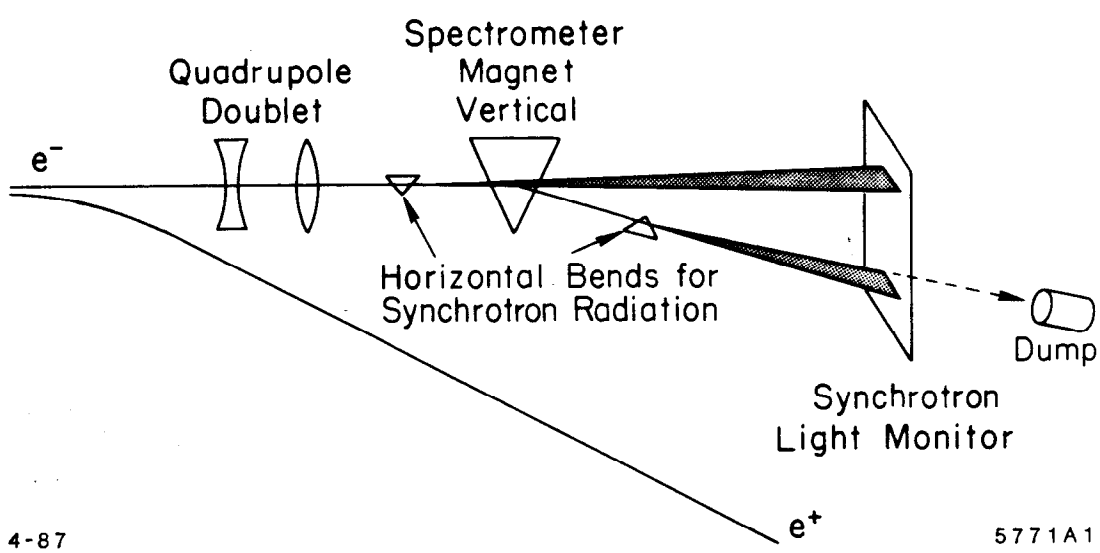
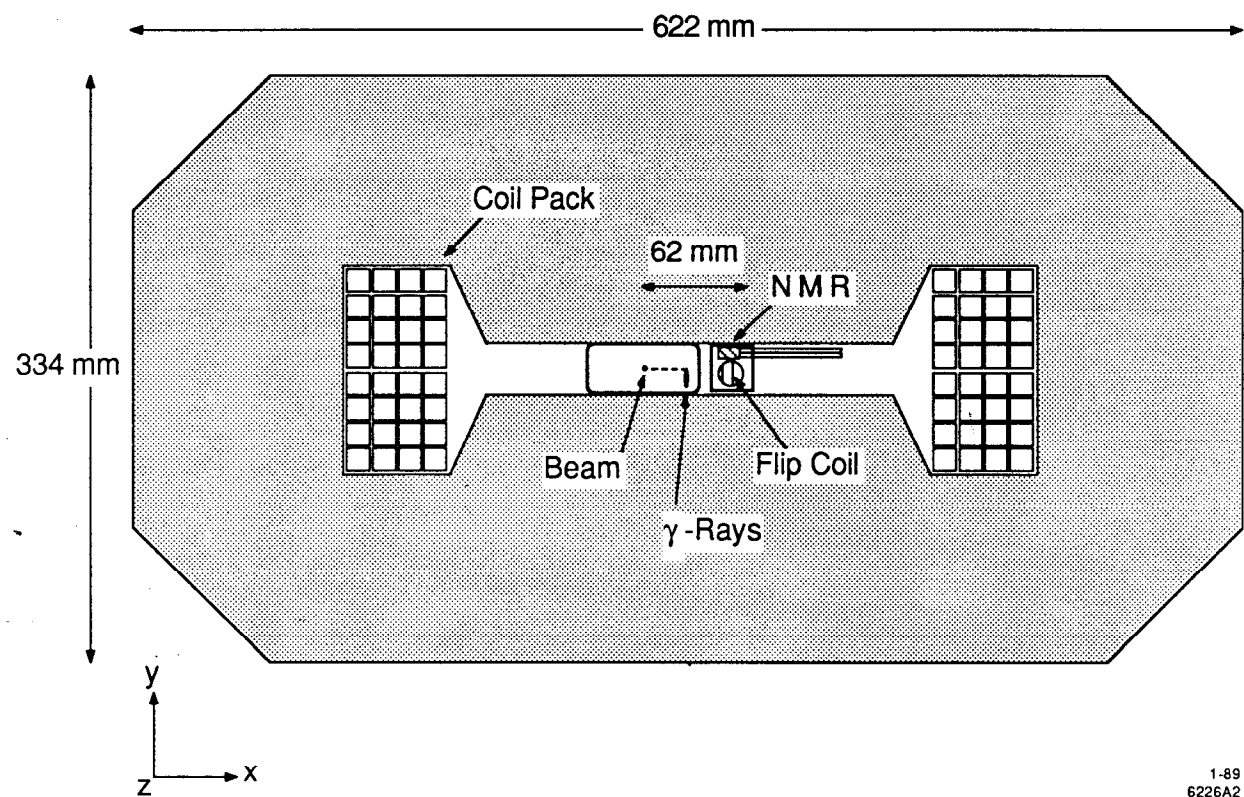


Fig. 1



1-89  
6226A2

Fig. 2

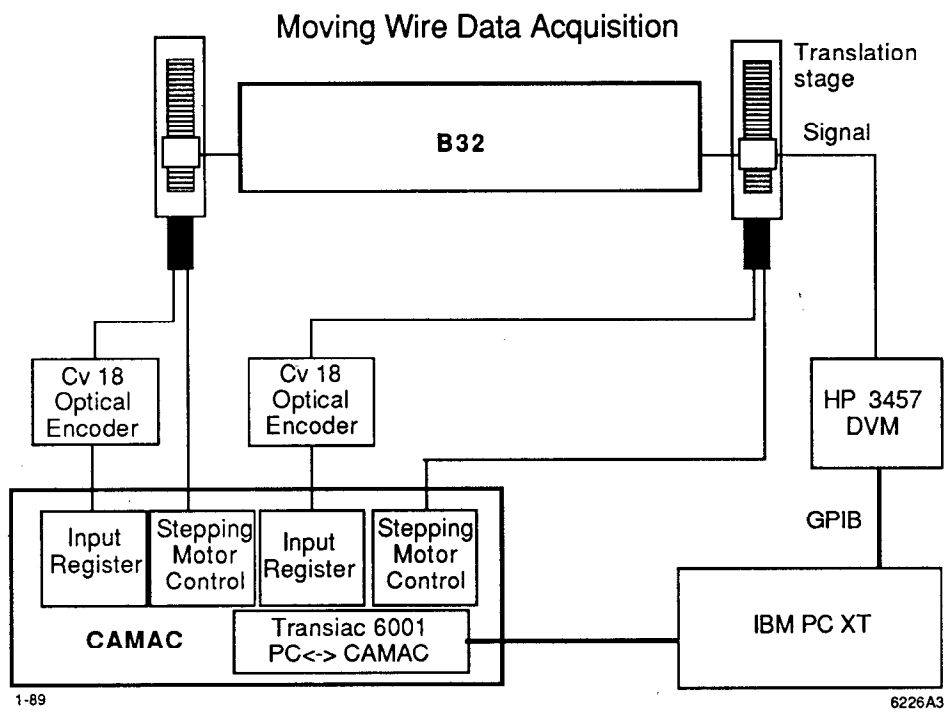
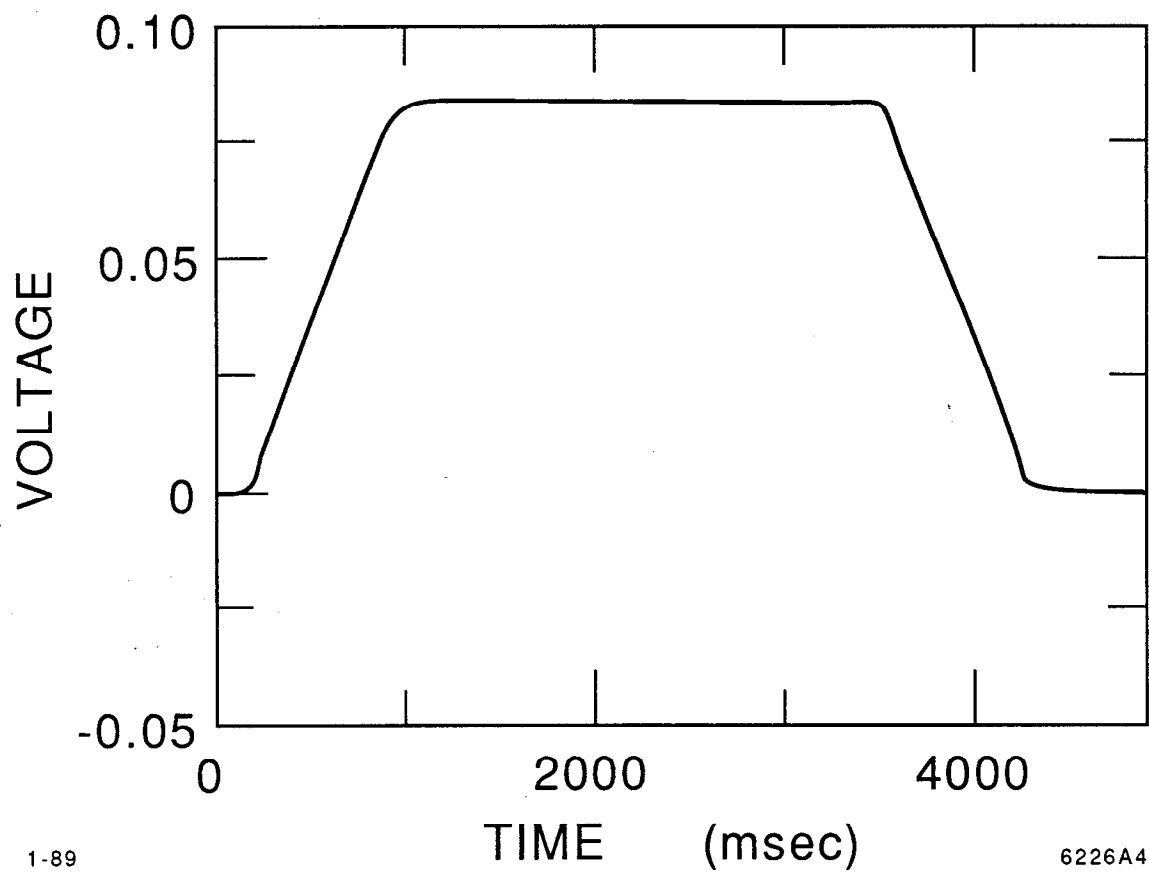


Fig. 3



1-89

6226A4

Fig. 4

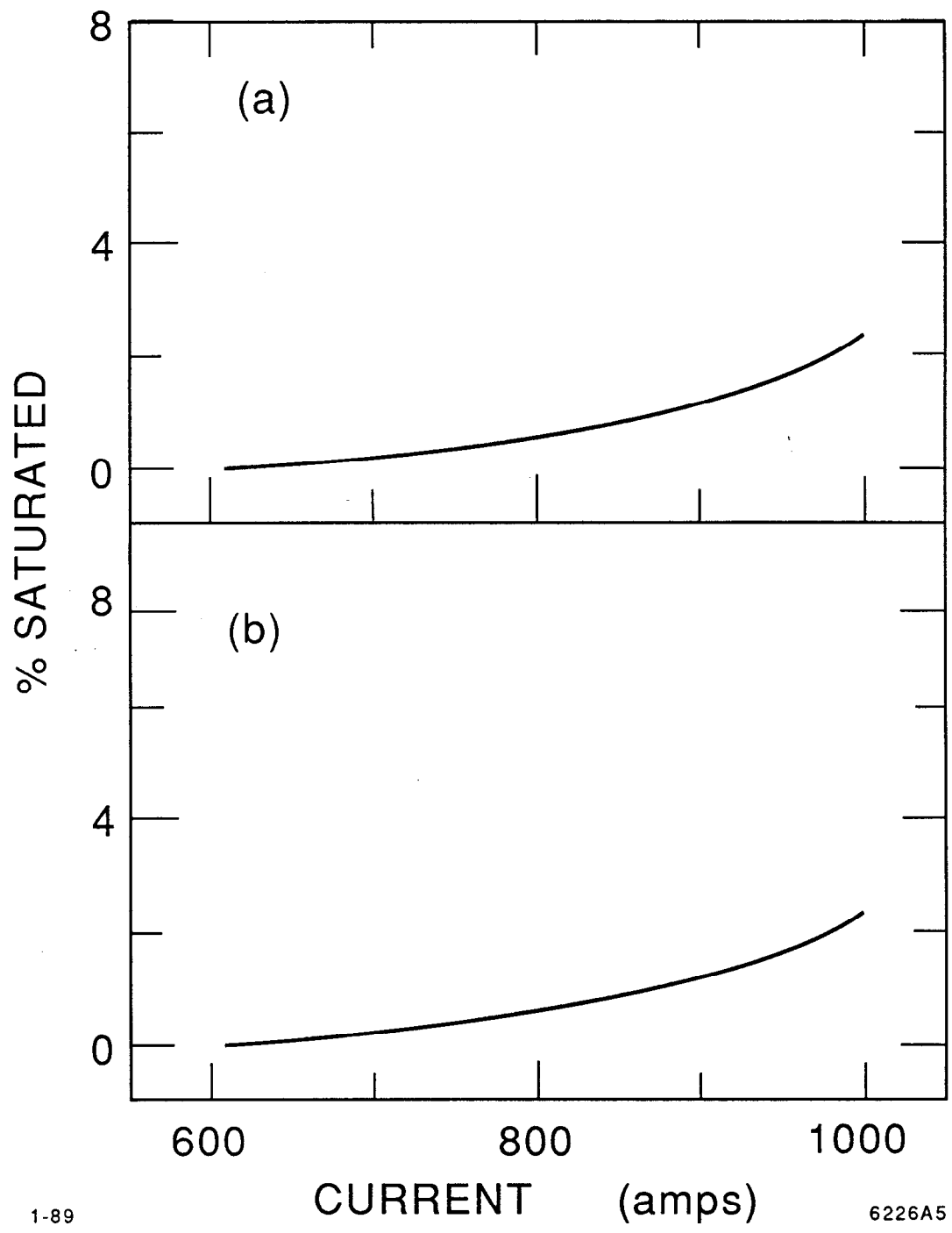


Fig. 5

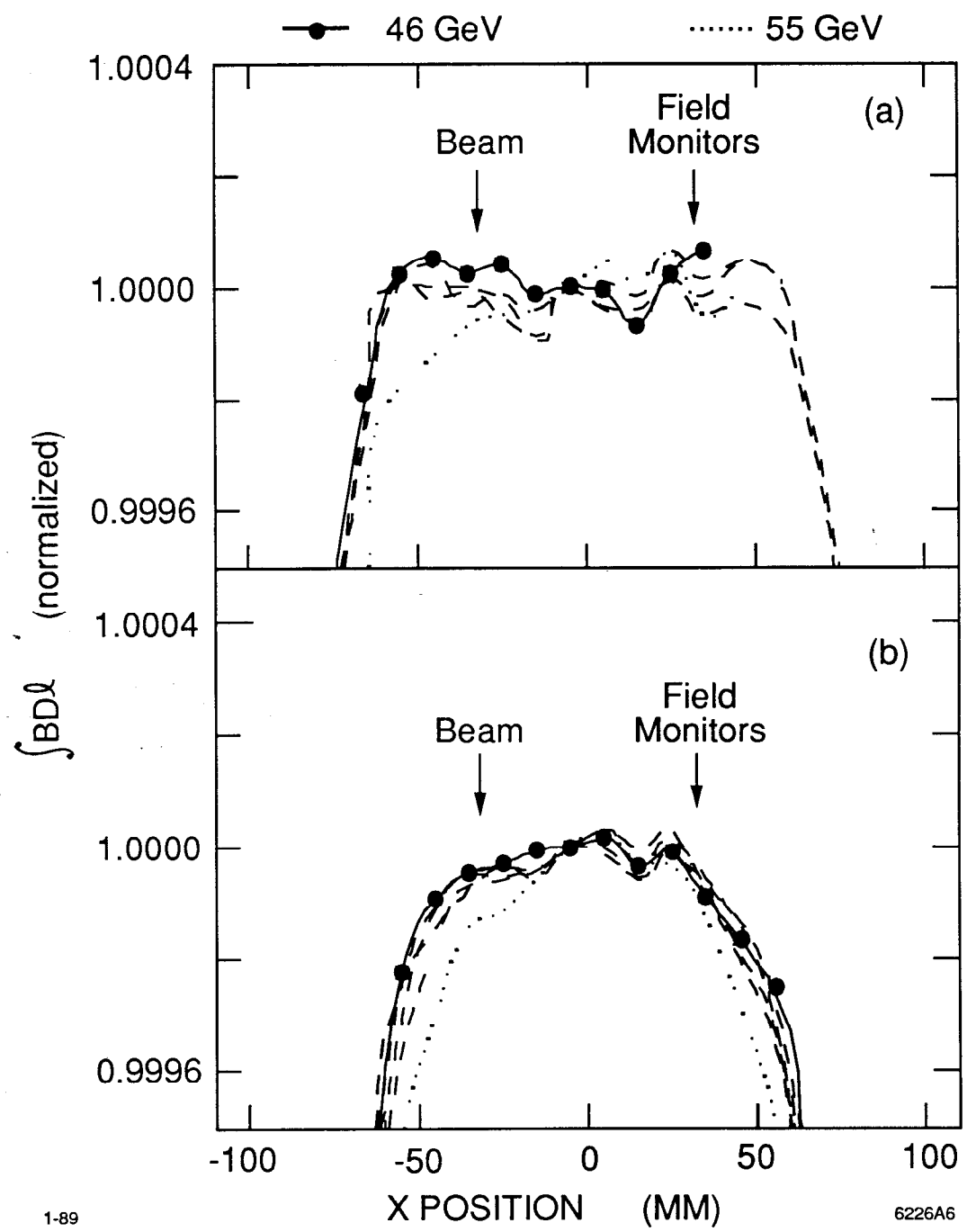


Fig. 6

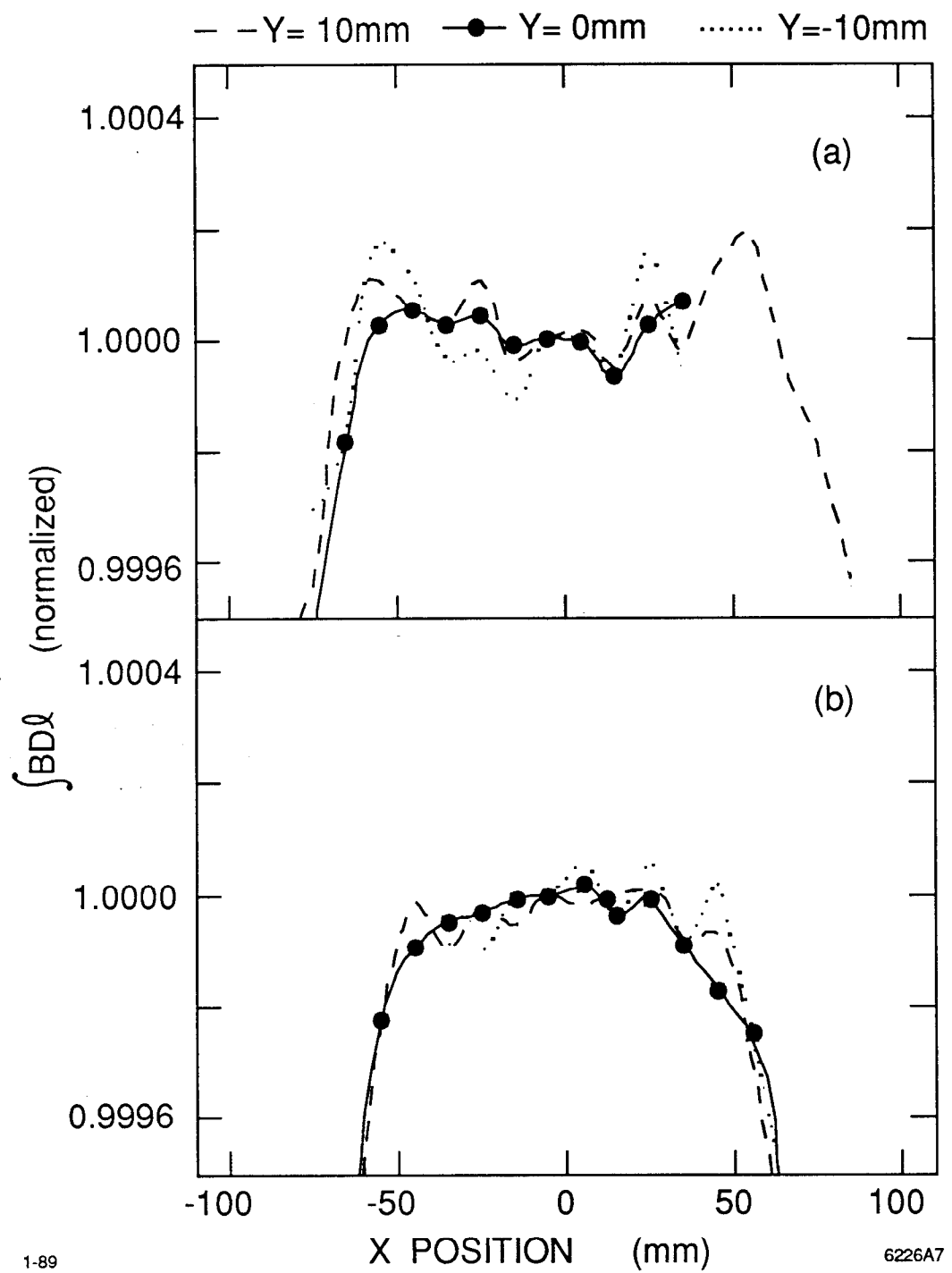


Fig. 7

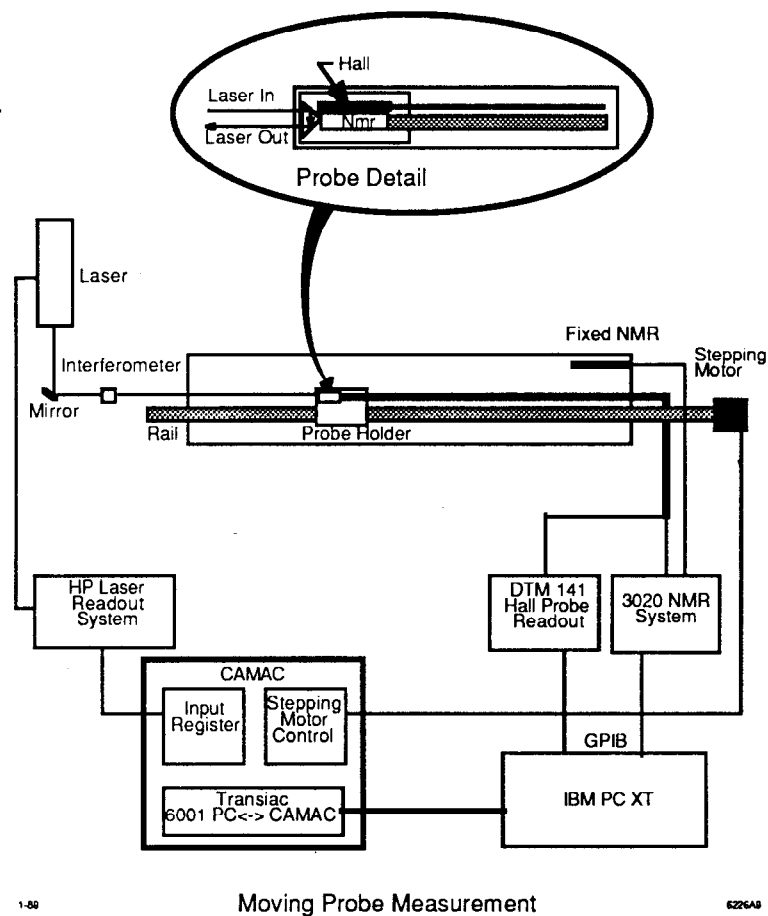


Fig. 8

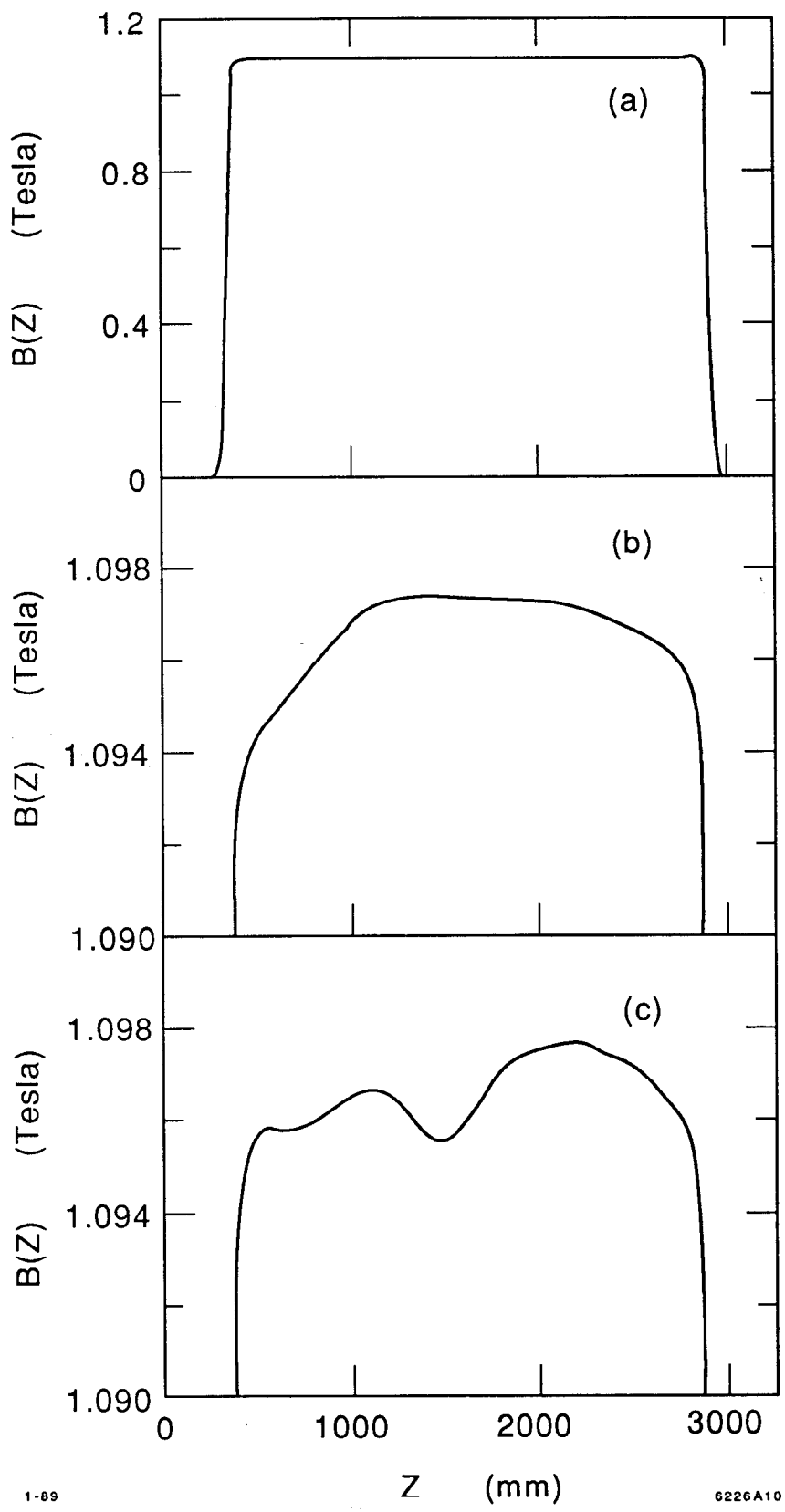


Fig. 9

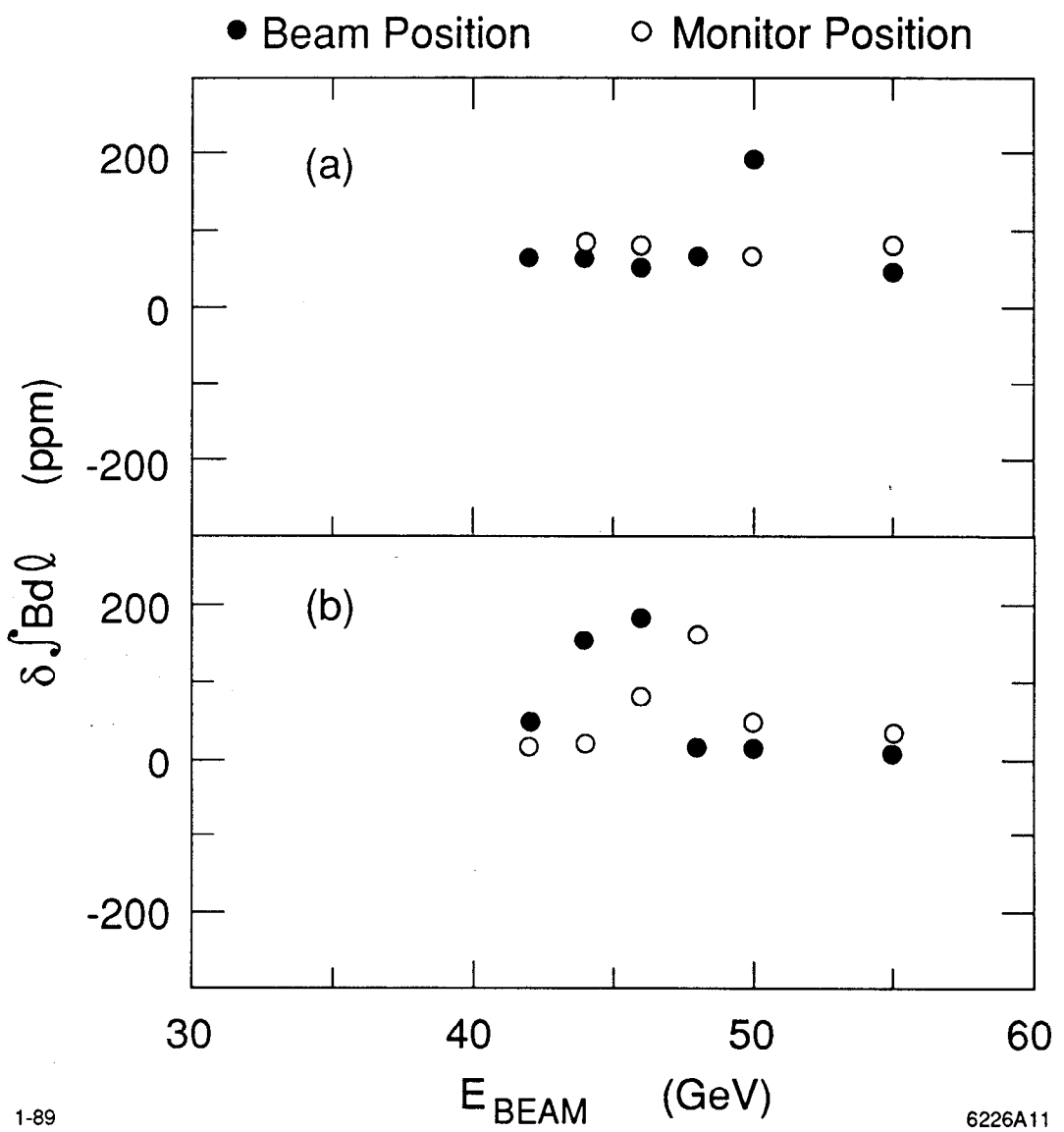
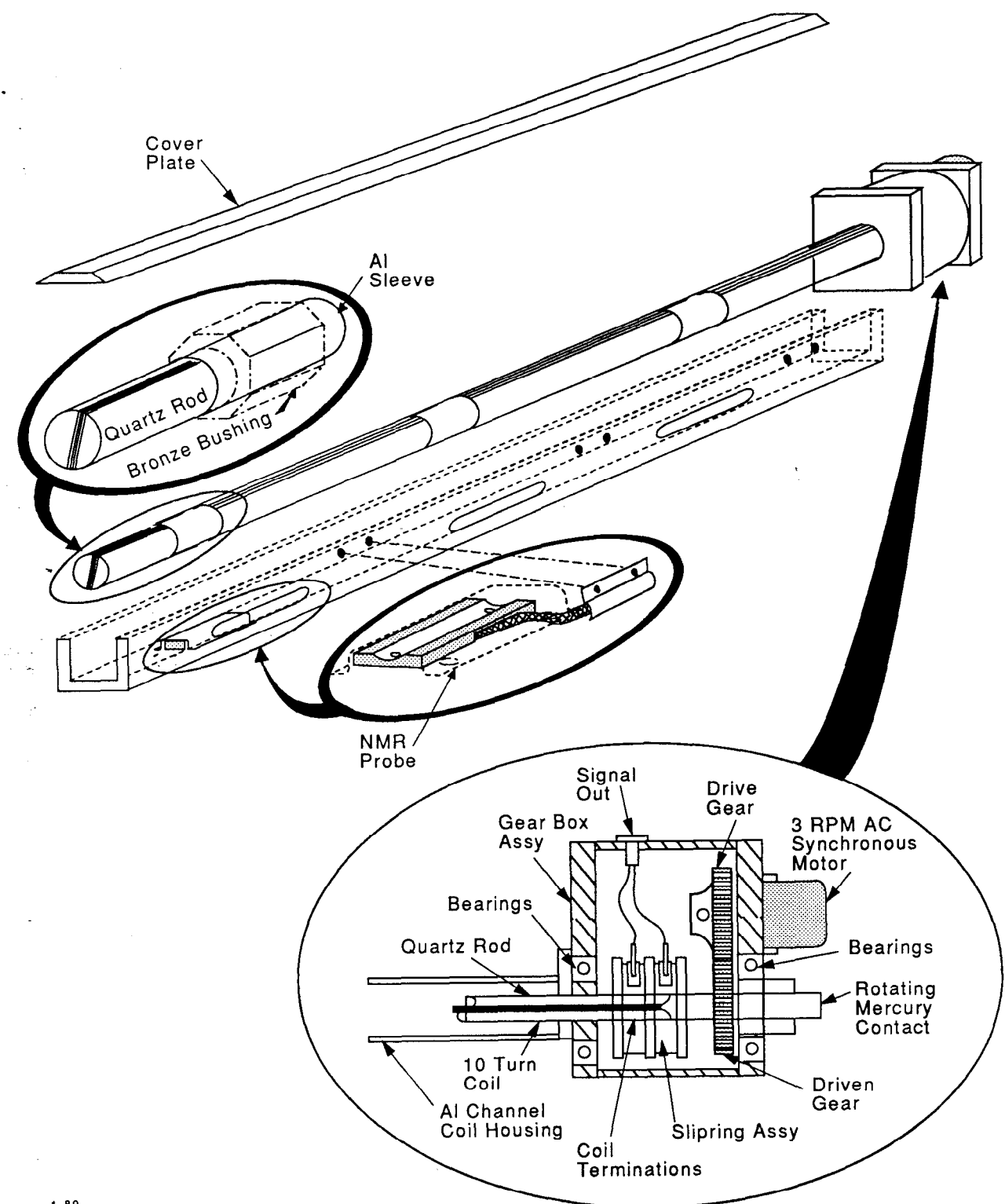
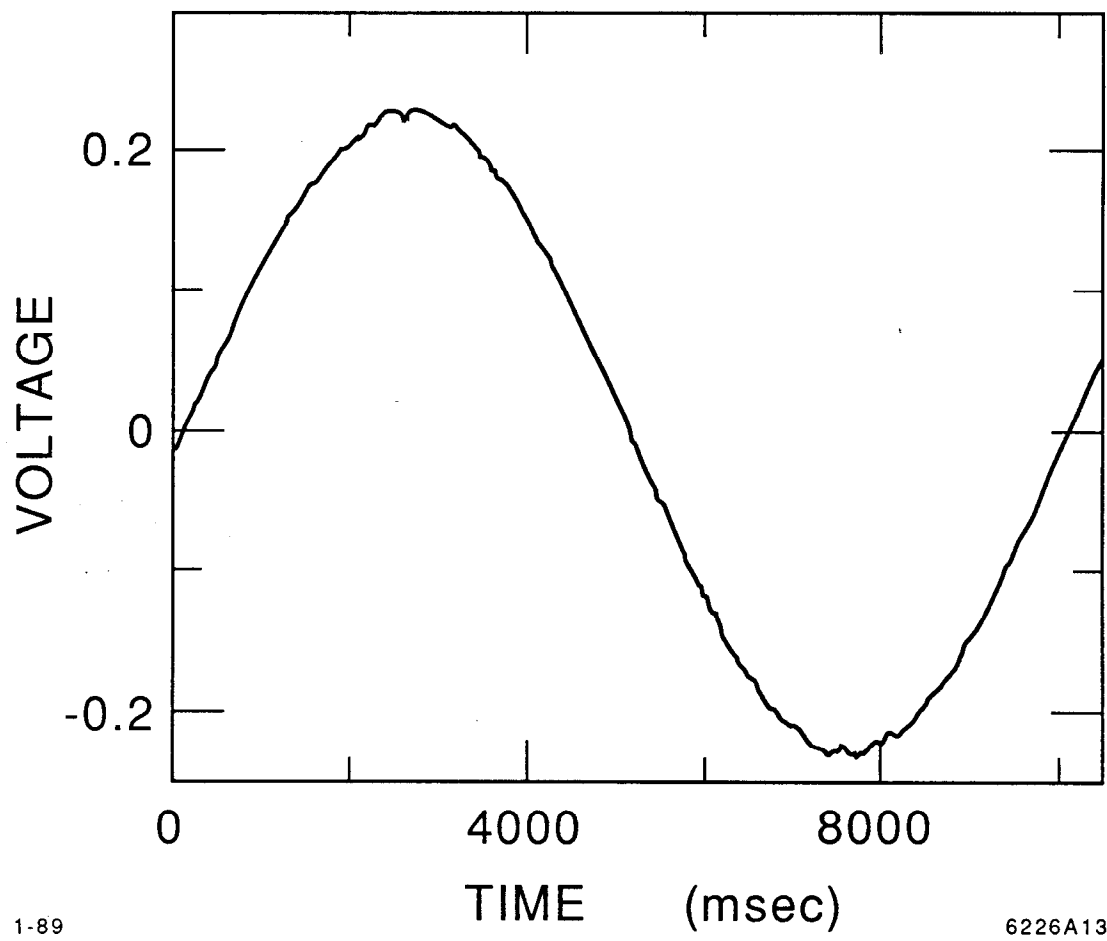


Fig. 10



1-89  
6226A12

Fig. 11



1-89

6226A13

Fig. 12

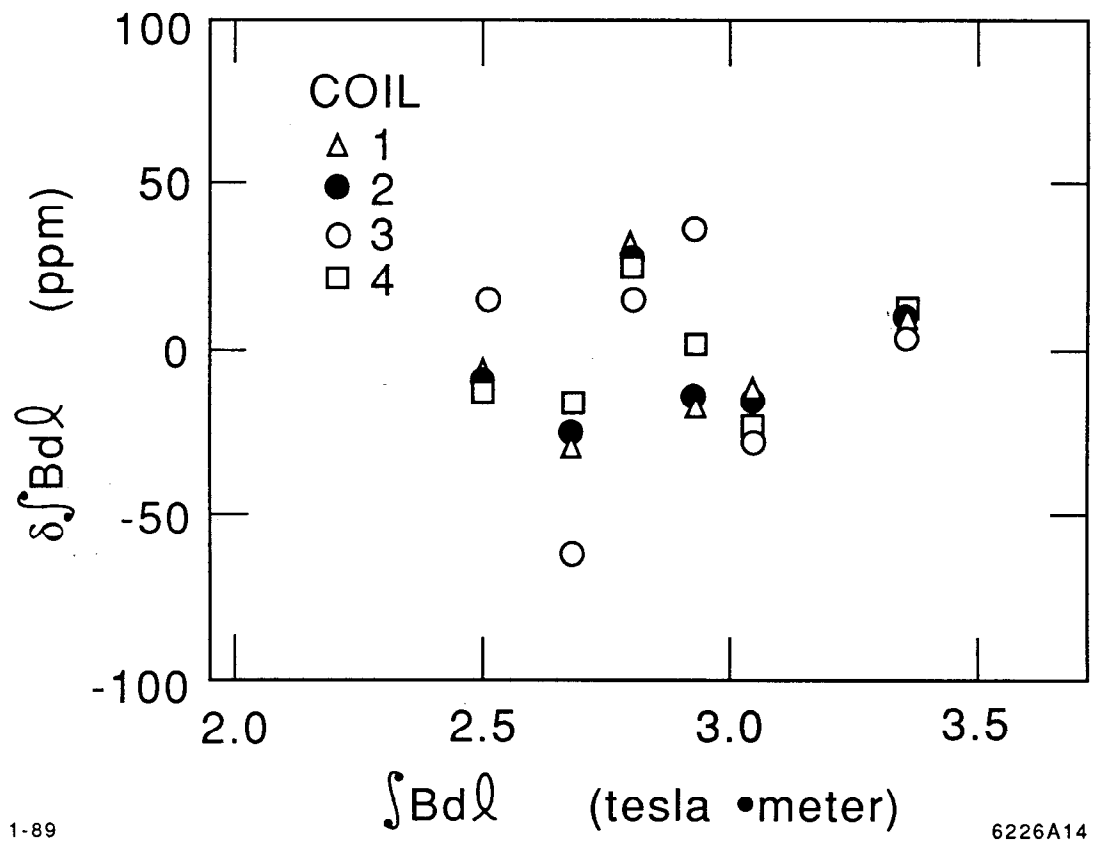


Fig. 13

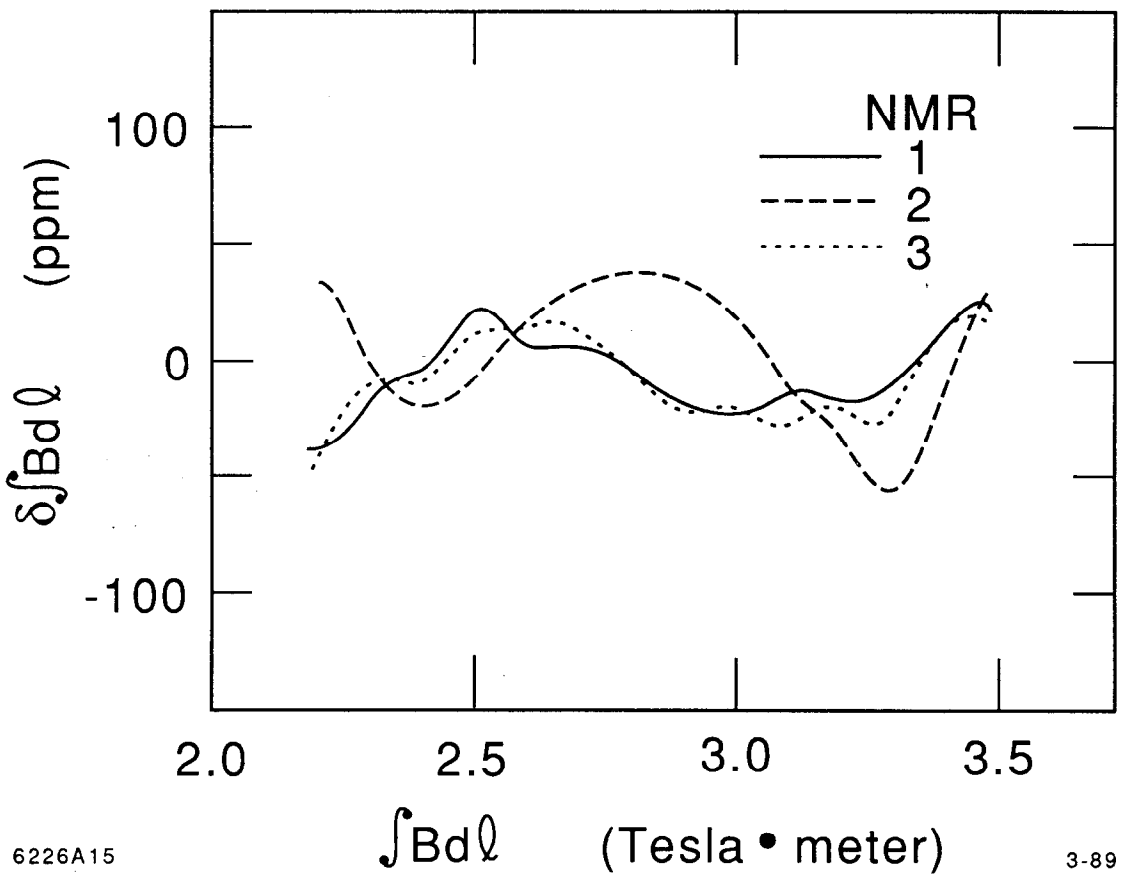


Fig. 14

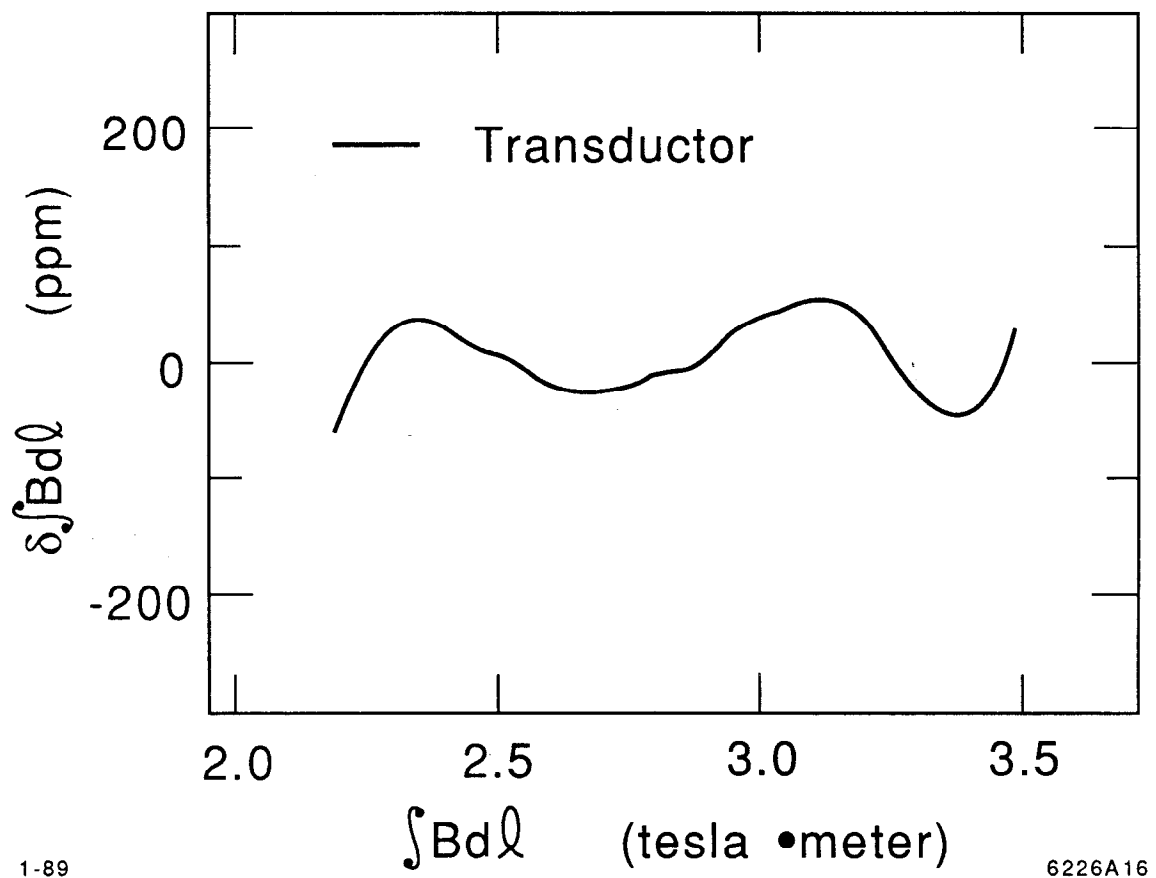


Fig. 15

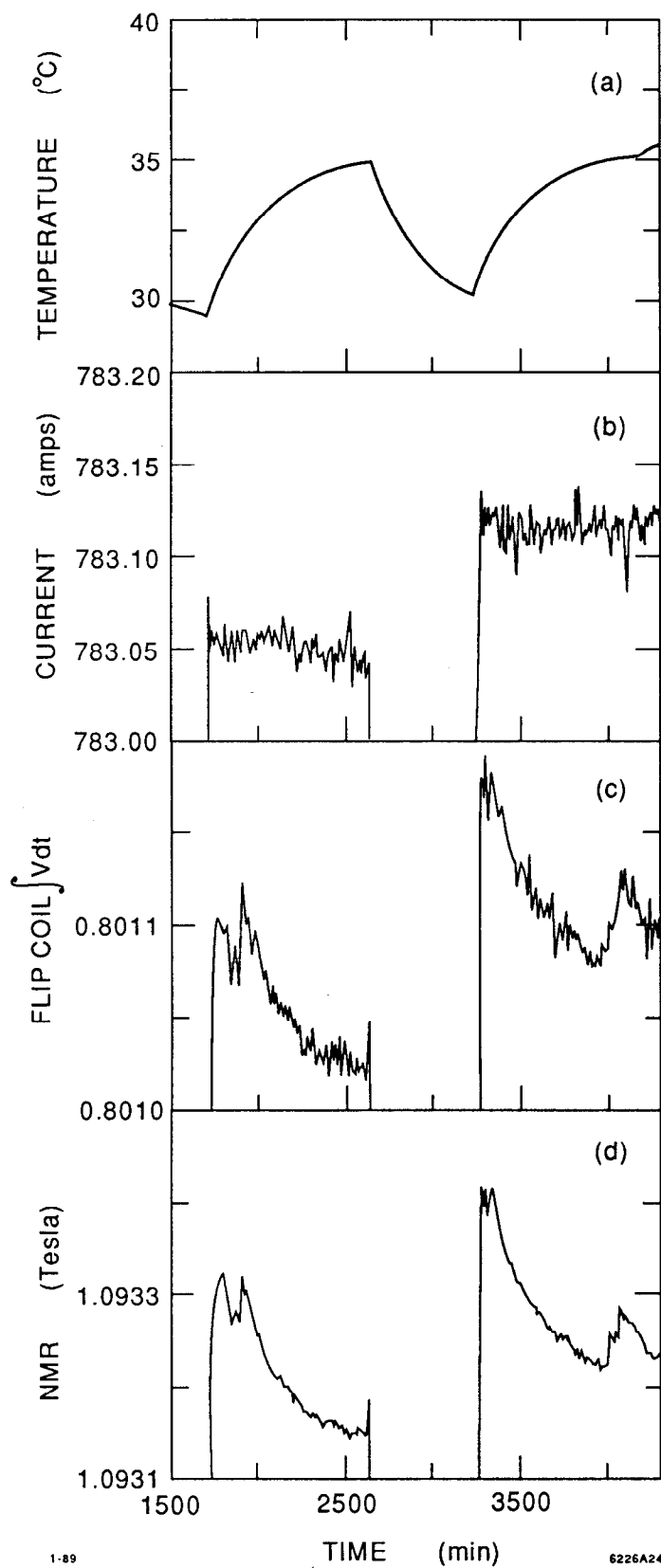


Fig. 16

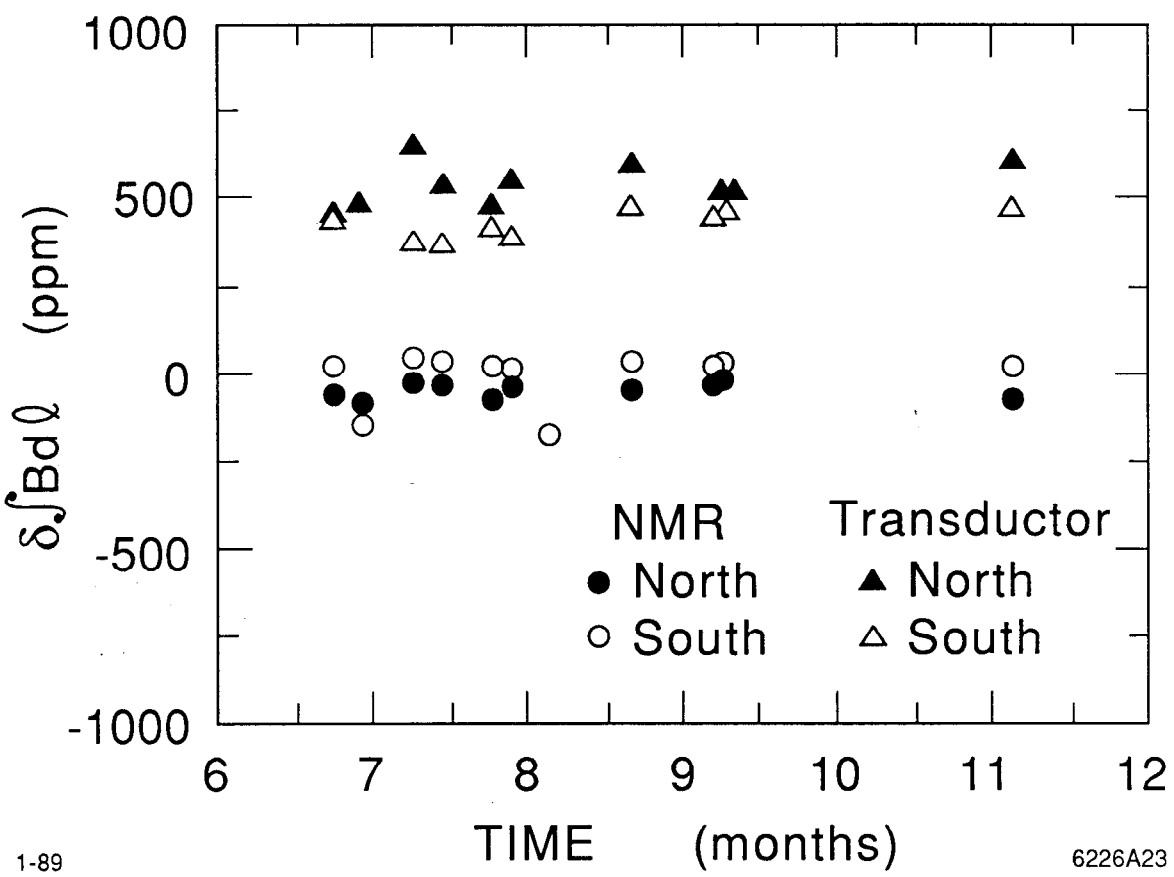


Fig. 17

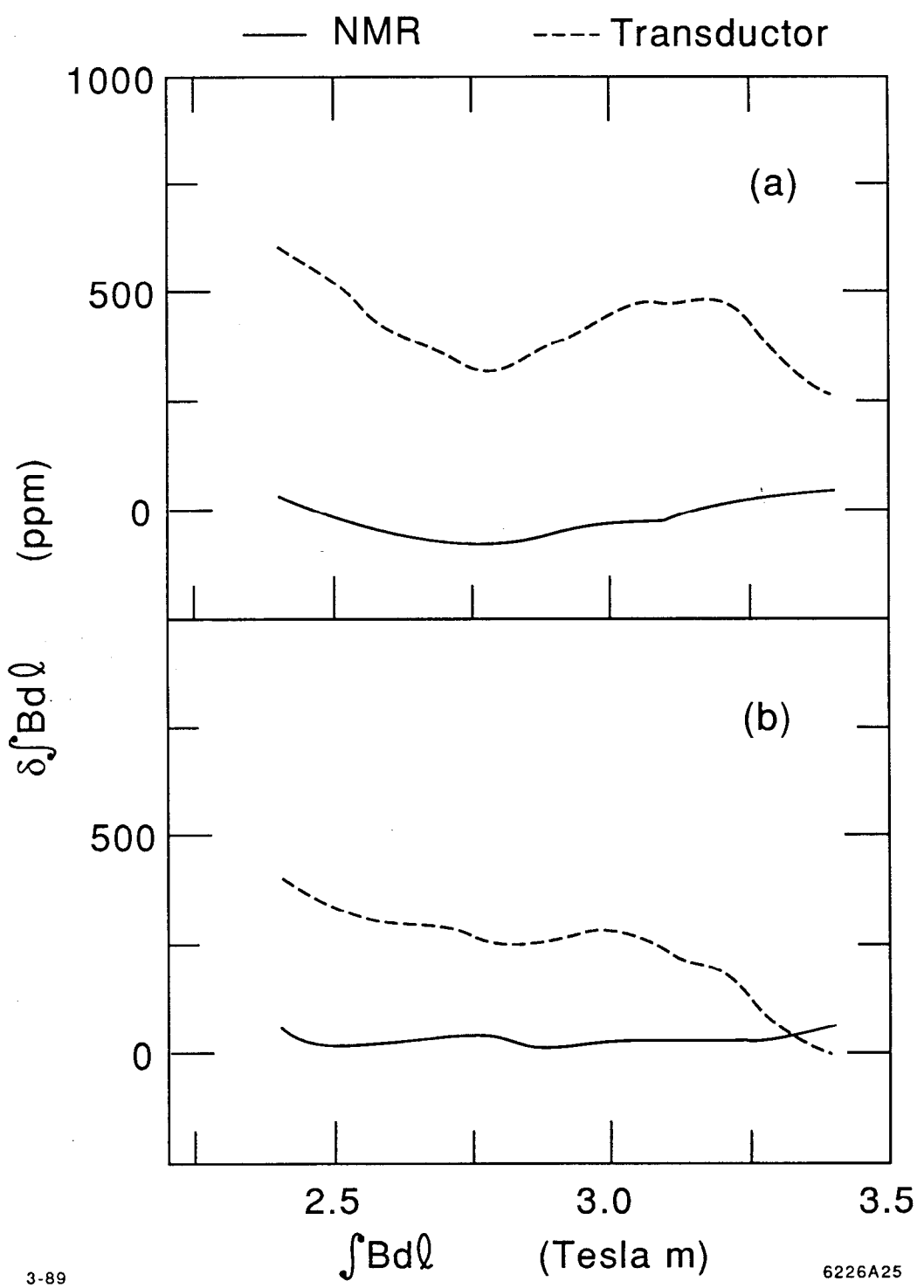


Fig. 18